Impact of a new H/He equation of state on the evolution of massive brown dwarfs

Gilles Chabrier, Isabelle Baraffe, Mark Phillips, Florian Debras

A&A 671, A119 (2023)
https://doi.org/10.1051/0004-6361/202243832

Astronomy & Astrophysics

Impact of a new H/He equation of state on the evolution of massive brown dwarfs

New determination of the hydrogen burning limit

Gilles Chabrier[1,2], Isabelle Baraffe[2,1], Mark Phillips[3,2], and Florian Debras[4]

[1] École normale supérieure de Lyon, CRAL, CNRS, UMR 5574, 69364 Lyon Cedex 07, France
e-mail: gilles.chabrier@ens-lyon.fr
[2] Physics & Astronomy Dpt, University of Exeter, Exeter EX4 4QL, UK
[3] Institute for Astronomy, University of Hawaii at Manoa, Honolulu, HI 96822, USA
[4] IRAP, Université de Toulouse, CNRS UMR 5277, UPS, Toulouse, France

Received 21 April 2022 / Accepted 19 November 2022

ABSTRACT

We explored the impact of the latest equation of state (EOS) for dense hydrogen–helium mixtures, which takes into account the interactions between hydrogen and helium species during the evolution of very low-mass stars and brown dwarfs (BDs). These interactions modify the thermodynamic properties of the H/He mixture, notably the entropy, a quantity of prime importance for these fully convective bodies, but also the onset and the development of degeneracy throughout the body. This translates into a faster cooling rate, that is, cooler isentropes for a given mass and age, and thus larger BD masses and smaller radii for a given effective temperature and luminosity than the models based on previous EOSs. This means that objects of a given mass and age in the range $M \lesssim 0.1\,M_{\odot}$, $\tau \gtrsim 10^8$ yr will have cooler effective temperatures and fainter luminosities. Confronting these new models with several observationally determined BD dynamical masses, we show that this improves the agreement between evolutionary models and observations and resolves at least part of the observed discrepancy between the properties of dynamical mass determinations and evolutionary models. A noticeable consequence of this improvement of the dense H/He EOS is that it yields a larger H-burning minimum mass, now found to be $0.075\,M_{\odot}$ ($78.5\,M_{\rm Jup}$) with the ATMO atmosphere models for solar metallicity. These updated BD models are made publicly available.

Key words. dense matter – equation of state – stars: low-mass – brown dwarfs

1. Introduction

Tremendous progress has been accomplished over the years in the theoretical description of brown dwarfs (BDs), enabling us to better understand their fundamental properties and cooling histories. The most recent developments include a more complete description of their atmosphere, and therefore of their spectral energy distribution (SED; e.g. Morley et al. 2012, 2014; Tremblin et al. 2015, 2016, 2017), and of their interior, notably concerning the equation of state (EOS) of dense hydrogen and helium (Chabrier et al. 2019, CMS19). A new generation of BD evolutionary models has recently been derived that incorporates both new (so-called ATMO) atmosphere models and the new CMS19 H/He EOS (Phillips et al. 2020). As shown in these models, a noticeable impact of this new EOS is that it yields denser and cooler – and therefore more degenerate – objects than those of the same mass computed with the Saumon–Chabrier–vanHorn (SCvH) EOS (Saumon et al. 1995). This yields slightly faster cooling rates and therefore cooler temperatures and lower brightness at a given age (Phillips et al. 2020).

Nevertheless, a puzzling issue has emerged within recent years as a result of the determination of the dynamical masses of several 'massive' T-dwarfs (Cheetham et al. 2018; Dieterich et al. 2018; Dupuy et al. 2019; Bowler et al. 2018; Sahlmann et al. 2020; Brandt et al. 2019). These observations reveal significantly larger dynamical masses than the theoretical predictions for the determined effective temperature and age. A common feature of all these objects is their relatively high mass (~60–75 $M_{\rm Jup}$), near the hydrogen-burning minimum mass (HBMM), similar spectral type (late T), and cool effective temperatures ($T_{\rm eff} \lesssim 1200$ K), which suggests ages in the range ~5–10 Gyr, and at the very least >1 Gyr. A noticeable exemple of this puzzling issue is the recent dynamical mass determination of Gliese 229 B, with a larger mass than estimated previously (Brandt et al. 2020). For all these late, massive T-dwarfs, all existing BD evolutionary models generally underpredict the mass for the nominal ages and temperatures, suggesting overly low cooling rates for these objects. This trend is confirmed by the recent thorough analysis of BD companion dynamical masses using HIPPARCOS and *Gaia* EDR3 data and age determinations based on activity–rotation–age calibrations by Brandt et al. (2021). For old ($\gtrsim$5 Gyr) and high-mass ($\gtrsim 60\,M_{\rm Jup}$) BDs, the models overpredict luminosities for the measured mass and age, or equivalently underestimate (overestimate) the mass (the age) for the correct age (mass). As noted by Dieterich et al. (2018), concerning the Eps Indi B-C system, models cannot make such massive objects reach such a cool $T_{\rm eff}$ within the age of the Galaxy. Due to the degeneracy between mass and age in the substellar domain, there are no reliable age indicators for isolated BDs, and therefore no robust constraint can be derived regarding substellar cooling rates and evolutionary models. In contrast, the aforementioned BD companions to

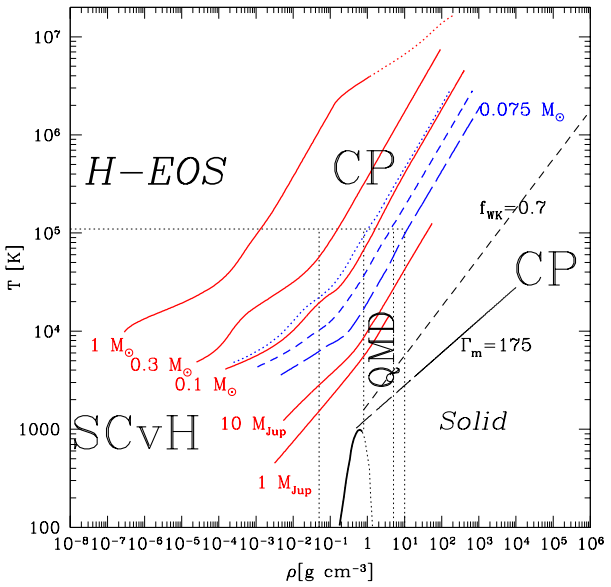

Fig. 1. Interior T–ρ profiles in the hydrogen phase diagram for different astrophysical bodies at about 5 Gyr, as labelled in the figure (red lines), and for a 0.075 $M_\odot$ object at 10^8, 8×10^8 and 8×10^9 yr (blue dotted, short-dashed and long-dashed lines, respectively). The SCvH, CP, and QMD labels stand for Saumon et al. (1995) EOS, Chabrier & Potekhin (1998) EOS, and QMD simulations. The line $f_{\rm WK}$ correponds to the onset of quantum (diffration) effects on the ions while $\Gamma_{\rm m}$ delineates the hydrogen melting line (see Chabrier et al. 2019 and Chabrier & Debras 2021 for details).

higher mass stars with masses close to the stellar-substellar limit allow us to test a boundary value of the theory of substellar structure and evolution.

A related diagnostic of these observations is the suggestion that the HBMM, identified as a minimum in the radius–effective temperature and radius–luminosity relations, is larger and lies at an effective temperature that is ∼400 K larger than predicted by all current models (Dieterich et al. 2014).

In this paper, we show that the most recent improvements in EOS calculations of dense hydrogen–helium mixtures contribute to resolving these issues in BD cooling theory. From a more general perspective, it should be mentioned that the aforementioned recent analysis of Brandt et al. (2021) suggests another, different issue for young (<1 Gyr) and low-mass ($\lesssim$40 $M_{\rm Jup}$) BDs. In that case, the trend is the opposite: models underpredict luminosities for any given mass and age, or equivalently overestimate (underestimate) the mass (the age) for the correct age (mass). For objects in between, that is, with mass ∼40–70 $M_{\rm Jup}$ and age ∼1–5 Gyr, models agree well ($<1\sigma$) with observations (see Table 10 of Brandt et al. 2021). This points to two different issues in BD cooling theory in the extreme mass and age limits. In the present paper, we focus on the first of these two issues, for which we show that part of the solution lies in the EOS. In contrast, the second problem is more likely to stem from remaining uncertainties in BD atmosphere models.

2. Impact of the new equations of state on the internal structure, cooling history, and hydrogen-burning limit

Figure 1 displays temperature–density profiles of various astrophysical bodies – from 1 $M_\odot$ to 1 $M_{\rm Jup}$ for an age of about 5 Gyr – in the phase diagram of hydrogen for the T–ρ range covered by the CMS19 and Chabrier & Debras (2021, CD21) EOSs. This diagram is similar to the ones portrayed in these latter papers for H and He and we refer the reader to these papers for more details. The key issue here is that, as illustrated by the central part of the diagram labelled QMD (which stands for quantum molecular dynamics), all BD cooling tracks enter the domain where interactions between H and He species can no longer be ignored, as assumed in the so-called ideal (or 'additive') volume law approximation used in CMS19 and Saumon et al. (1995, SCvH) (see Fig. 1 of CD21 for further details). Recently, Chabrier & Debras (2021) took into account the impact of these interactions on the thermodynamic properties of the H–He mixture by incorporating the QMD calculations performed by Militzer & Hubbard (2013) into the EOS. Figure 1 also displays the cooling sequence of a 0.075 $M_\odot$ object at 10^8, ∼10^9, and ∼10^{10} yr, respectively. As seen in the figure (see also the conclusions of CMS19), essentially all objects below 0.1 $M_\odot$ older than about ∼0.1 Gyr will enter the domain where H–He interactions cannot be ignored and will affect their mechanical and thermal properties to some degree, and therefore their structure and evolution. It is the aim of the present paper to examine this impact in detail.

The left panel of Fig. 2 displays the evolution of the central density, $\rho_{\rm c}$, temperature, $T_{\rm c}$, and degeneracy parameter, $\psi_{\rm c} = (T_{\rm c}/T_{\rm F}) \approx 3.314 \times 10^{-6} T_{\rm c}(\mu_{\rm e}/\rho)^{2/3}$, where $T_{\rm F}$ and $\mu_{\rm e}$ denote the electron *Fermi* temperature and mean molecular weight, respectively, of a 0.075 $M_\odot$ object (see Chabrier & Baraffe 2000). The evolution is calculated with our recent so-called ATMO atmosphere models and updated solar abundances (Caffau et al. 2011) for a global helium and heavy element abundance $Y = 0.275, Z_\odot = 0.017$, respectively (Phillips et al. 2020), but with three different H–He EOSs, namely those of Saumon et al. (1995, SCvH), Chabrier et al. (2019, CMS19), and Chabrier & Debras (2021, CD21). The differences between these different EOSs, and the improvements in the treatment of the H–He interactions, are described in detail in these papers. As already mentioned in Phillips et al. (2020) and Chabrier & Debras (2021) and clearly seen in Fig. 2, the new EOSs yield denser and cooler structures for a given object, and therefore more correlated and degenerate (lower ψ) interiors. This in turn increases the cooling rate of the object. This is illustrated in the right panel of Fig. 2, which portrays the late evolution of the effective temperature, luminosity, and radius of objects of 0.073 (black), 0.074 (blue), and 0.075 (red) $M_\odot$ for the same three EOSs. While these three quantities, notably $T_{\rm eff}$ and L, become constant after $\sim 5 \times 10^8$ yr at 0.073 $M_\odot$ with the SCvH EOS, indicating the stellar–substellar boundary, they continue to decrease with the two other EOSs, with this limit occuring at 0.074 $M_\odot$ with the CMS19 EOS and at 0.075 $M_\odot$ with the CD21 EOS. Table 1 displays the characteristics of the steady H-burning limit (HBL) obtained with the three EOSs. We define the HBL as the limit below which nuclear equilibrium ($L_{\rm nuc} = L_\star$) will never be reached, and therefore below which cooling and gravitational contraction will continue indefinitely. This corresponds to the physical limit of the stellar main sequence, that is, the stellar–substellar boundary. Any object below this limit, that is, cooler and fainter than the corresponding effective temperature and luminosity (see Table 1), will be a brown dwarf, whatever its age. However, we note that the opposite is not true: objects hotter and brighter than these limits can be either stars or BDs, depending on their age. The H-burning minimum mass (HBMM), which is the minimum mass to sustain hydrogen fusion, and which does not depend on the age, is found to be 0.075 $M_\odot$ (∼78.5 $M_{\rm Jup}$) with the most recent CD21 EOS. For the sake of comparison, this table also provides the characteristics of the HBL obtained by Baraffe et al. (2003). These models use the

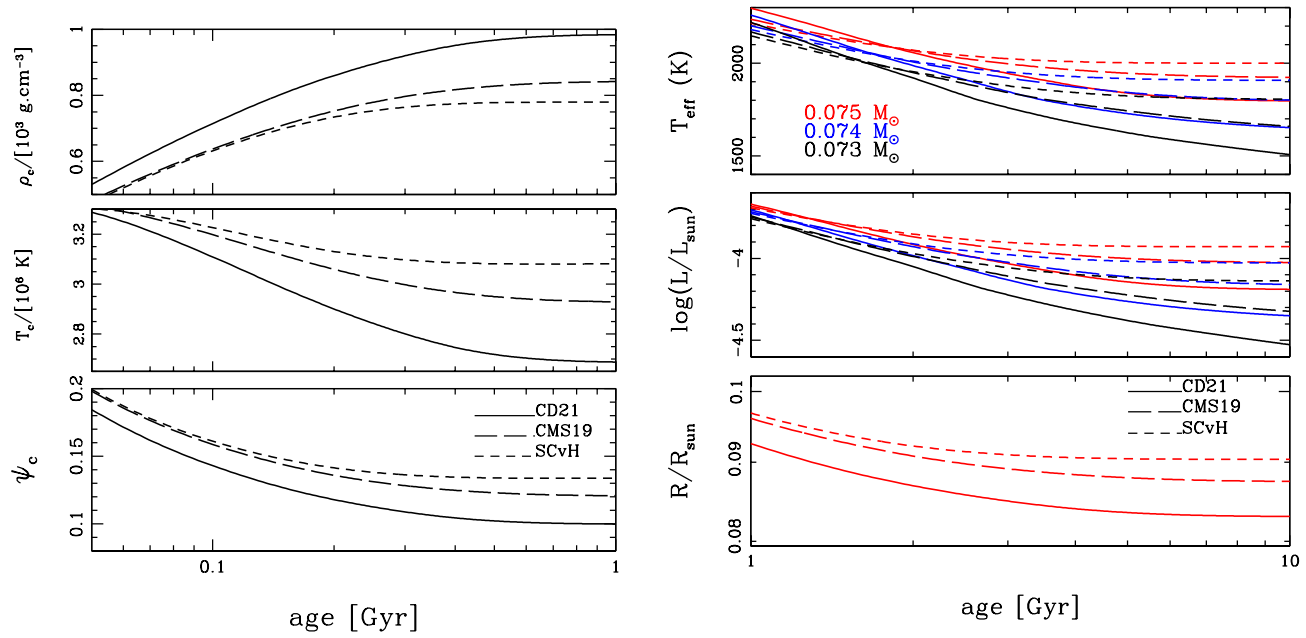

Fig. 2. Impact of the EOS on the evolution. Left: evolution of the central density, temperature, and degeneracy parameter for a 0.075 $M_\odot$ object calculated with three different EOSs, namely CD2021 (solid line), CMS2019 (long-dashed line), and SCvH (dotted line). Right: evolution of the effective temperature and luminosity for 0.075 (red), 0.074 (blue), and 0.073 (black) $M_\odot$ and radius for 0.075 $M_\odot$, with the same three EOSs.

Table 1. Mass, effective temperature, luminosity, and radius characteristic of the H-burning limit (t = 10 Gyr) with the Saumon et al. (1995), Chabrier et al. (2019) and Chabrier & Debras (2021) EOSs, all calculated with the ATMO atmosphere models.

EOS	$M_{\rm HBMM}/M_\odot$	$T_{\rm eff\,HBL}$ [K]	$\log(L/L_\odot)_{\rm HBL}$	$R_{\rm HBL}/R_\odot$
SCvH+COND (Baraffe et al. 2003)	0.072	1560	−4.47	0.081
SCvH+ATMO	0.073	1807	−4.14	0.087
CMS'19+ATMO (Phillips et al. 2020)	0.074	1800	−4.16	0.085
CD'21+ATMO (present)	0.075	1800	−4.19	0.083

Notes. For the sake of comparison, the results with the COND atmosphere models are also presented.

SCvH EOS, and the same helium and heavy element abundances as mentioned above but the so-called COND model atmospheres. These comparisons enable us to disentangle the impacts of the atmosphere and EOS models, respectively, on the cooling properties of an object at the H-burning limit. The atmosphere models have been greatly improved between the COND and ATMO models. Line opacities, in particular, were missing in the former, yielding a much faster cooling rate and therefore explaining the cooler and fainter limits at the HBL. However, the EOS also bears some impact on the HBL. As seen in Table 1, the higher cooling rate with the new EOS translates into a larger HBMM with a smaller radius than in the previous calculations. On the other hand, the luminosities at the HBL remain barely affected ($\lesssim$10%) and the effective temperature remains essentially the same. This is explained by the fact that the threshold for hydrogen fusion at the centre of the star occurs at a fixed temperature and therefore for the same interior–atmosphere (T_c–$T_{\rm eff}$) boundary condition, at the same effective temperature. In contrast, the nuclear energy rate, and therefore the luminosity, depends on the mass and then slightly differs between the three different HBMMs.

On the other hand, Dieterich et al. (2014) determined the effective temperature and bolometric fluxes of 63 objects ranging in spectral type from M6V to L4, bracketing the stellar–substellar boundary, by comparing observed optical and infrared photometric colours on nine bands with synthetic colours derived from the so-called BT-Settl model atmospheres (Allard et al. 2012, 2013) used in the Baraffe et al. (2015) evolutionary calculations. The optimisation procedure for determining effective temperatures also indicates which model spectrum in the BT-Settl grid provides the overall best fit to the observed photometry. Once the effective temperatures and bolometric fluxes of the objects were determined by this procedure, the radii of the objects with known trigonometric parallax were determined from the Stefan-Boltzmann law (see Dieterich et al. 2014 for details). As the differences between stellar and substellar objects become more pronounced at ages >1 Gyr, objects with known youth signatures were rejected from the sample. Based on this analysis, Dieterich et al. (2014) find evidence for a local minimum in the radius–temperature and radius–luminosity trends that indicates the vicinity of the stellar main sequence–BD sequence boundary (see e.g., Burrows et al. 1997; Chabrier & Baraffe 2000; Chabrier et al. 2009) at $T_{\rm eff\,HBL} \simeq$ 2075 K, $\log(L/L_\odot)_{\rm HBL} \simeq -3.9$, and $R/R_\odot \simeq 0.086$. The inversion of the radius trend occurs near the location of the L2.5 dwarf 2MASS J0523−1403 ($M = 67.54 \pm 12.79\,M_{\rm Jup}$, $Sp = L2.5$) (Filippazzo et al. 2015). Although at first glance this seems to point to a disagreement with the models in the determination of the HBL, it must be kept in mind that the age of the objects in the Dieterich et al. (2014) sample, although supposedly larger than

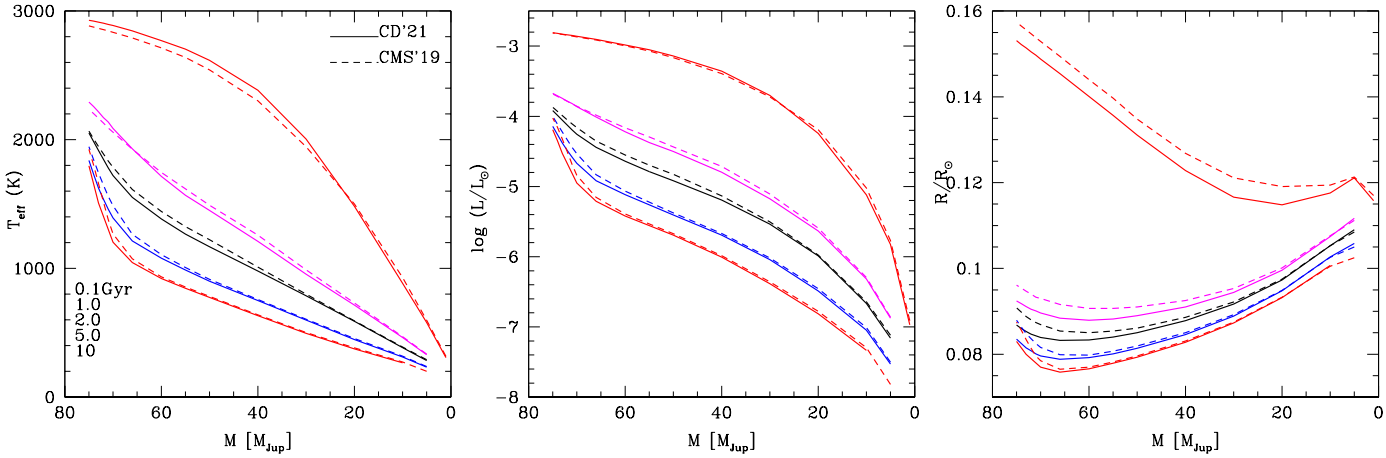

Fig. 3. Effective temperature, luminosity and radius for $M \leq 0.075\,M_\odot$ for 0.1, 1, 2, 5 and 10 Gyr (from top to bottom), respectively, for the same atmosphere models and helium and heavy element compositions but 2 different EOSs, namely Chabrier & Debras (2021) (present) and Chabrier et al. (2019) (Phillips et al. 2020).

1 Gyr, is unknown. This inevitably translates into some uncertainty in the comparison between observations and evolutionary calculations. However, as seen in the right panel of Fig. 2, the HBL is only reached at much older ages, namely of about 10 Gyr with the new EOS. Therefore, most of the objects identified in Dieterich et al. (2014), which lie at less than 25 pc and belong dominantly to the young disk, are too young to yield a proper determination of the HBL. On the other hand, as seen in Fig. 3, which portrays the $T_{\rm eff}$–M, L–M, and R–M relations below the HBMM for five isochrones, an average age of about 2 Gyr for the observed sample near the R–$T_{\rm eff}$ and R–L minimum location leads to excellent agreement between the observational determinations and the new models. As highlighted in the rightmost panel of Fig. 3, the minimum in the radius–mass relation does not occur exactly at the HBMM but at about 65 $M_{\rm Jup}$ (see e.g., Fig. 1 of Chabrier et al. 2009), which is consistent with the aforementioned BD 2MASS J0523−1403 determination, and is increasingly pronounced as objects get older. We see from the three panels that the observational identifications of the minimum radius in the sample of Dieterich et al. (2014) are consistent with objects of masses of ∼0.065−0.075 $M_\odot$ and ages of ∼1–2 Gyr. We also see that, whereas the newest EOS only modestly influences the effective temperature and the luminosity for a given mass and age compared with the CMS19 EOS used in the models of Phillips et al. (2020), it has a much greater impact on the radius, notably for the most massive BDs. This reflects the different rate at which degeneracy progresses throughout the body, starting at about ∼0.1 Gyr, as seen in the left panel of Fig. 2. The Phillips et al. (2020) models have been updated accordingly and are available online (see at the end of the paper).

It is important to mention at this stage that the procedure used by Dieterich et al. (2014) remains dependent on the model atmosphere, notably in a temperature domain characterised by cloud condensation and sedimentation in the models. Even though the BT-Settl atmosphere models used by Dieterich et al. (2014) have been shown to provide a remarkable agreement with observed M and L spectra, alternative 'cloudless' models have been proposed that are very successful in reproducing BD atmosphere spectra (Tremblin et al. 2015, 2016, 2017). 'Cloudless' in these models does not mean that clouds do not form, but rather that they are not responsible for shaping the spectral evolution of BDs. Instead, the (massive) BD spectral evolution is due to a thermo-compositional instability triggered by the chemical conversion CO → CH_4 in their atmospheres (Tremblin et al. 2019).

Concerning the domain of very-low mass stars (VLM, $M \leq 0.4\,M_\odot$) on the main sequence (age $\gtrsim$1 Gyr), the impact of the new EOS (CD21) compared with the SCvH one used in the Baraffe et al. (2015, BHAC) models is quite modest and is therefore not displayed here.

3. Comparison with the data

As mentioned in the previous section, near-infrared spectroscopic and imaging surveys have uncovered a population of short-period spectral binaries composed of low-mass stars and BDs, allowing precise dynamical determination of the mass of these latter objects. Activity and kinematic constraints on the age of the primary of these massive T-dwarfs lead to a range of 2–8 Gyr. In this section, we compare the effective temperatures obtained with the COND models (Baraffe et al. 2003) and the Phillips et al. (2020) models – based on the Chabrier et al. (2019) EOS–, and a subset of models based on the most recent Chabrier & Debras (2021) EOS, with the various observations of BD dynamical systems.

3.1. HD4113C

Using high-contrast imaging with the SPHERE instrument at the VLT, Cheetham et al. (2018) obtained the first images of the cold BD HD4113C ($Sp = T9$), which is part of a dynamical system with an M-dwarf companion. The dynamical mass is $M_{\rm dyn} = 66 \pm 5\,M_{\rm Jup}$, while comparison of the observed spectrum of HD4113C with atmospheric models (Morley et al. 2012, 2014; Tremblin et al. 2015) yields $T_{\rm eff} \sim$ 500–600 K, log g = 4.5–5.0, and a radius $R \sim 1.4$–$1.5\,R_{\rm Jup}$, which are much larger than predicted for old high-mass BDs. Using stellar evolution models (Mowlavi et al. 2012), the derived age of the parent star is found to be $\tau = 5^{+1.3}_{-1.7}$ Gyr. The COND models (Baraffe et al. 2003) for such temperatures predict a mass of $M = 36 \pm 5\,M_{\rm Jup}$ for the BD, in strong conflict with the dynamical mass. Conversely, for $M = 66\,M_{\rm Jup}$, these models predict $T_{\rm eff} \sim 1200 \pm 170$ K at the age of the system, which is significantly higher than the aforementioned estimates from the best-fit spectral models. Table 2 displays the temperature, luminosity, and radius obtained with the Phillips et al. (2020) models, which use the CMS19 models,

Table 2. Effective temperature, luminosity and radius of the various BDs examined in the text obtained with the P2020 and present models for the observed masses and ages.

Object		M [$M_{\rm Jup}$]	Age [Gyr]	$T_{\rm eff}$ [K]	$\log(L/L_\odot)$	$R/R_\odot$
HD4113C	Observations[(1,8)]	66±5	$5^{+1.3}_{-1.7}$	500–600	−6.30 ± 0.22	
	P2020	63	5	1108	−5.06	0.080
		66		1149	−4.99	0.080
	Present	63	5	1081	−5.11	0.079
		66		1144	−5.02	0.079
Eps Indi Ba	Observations[(2)]	66.92±0.36	$3.5^{+0.8}_{-1.0}$			
	Observations[(5)]	68±0.9		1312±9	−4.70±0.02	
	P2020	66–67	3.0	1324–1395	−4.72 – −4.63	0.083
			3.5	1262–1325	−4.81 – −4.73	0.082
			3.8	1233–1293	−4.85 – −4.78	0.081
	Present	66–67	2.8	1321–1354	−4.74 – −4.70	0.081
			3.0	1291–1321	−4.78 – −4.74	0.081
			3.5	1241–1265	−4.86 – −4.83	0.080
Eps Indi Bb (or C)	Observations[(2)]	53.25±0.29	$3.5^{+0.8}_{-1.0}$			
	Observations[(5)]	53±0.3		975±11	−5.23±0.02	
	P2020	53	3.0	1071	-5.08	0.084
			3.5	1023	−5.17	0.083
			3.8	996	−5.21	0.083
	Present	53	2.8	1060	−5.10	0.083
			3.0	1042	−5.13	0.083
			3.5	998	−5.22	0.083
			3.8	973	−5.26	0.082
GL 758 B	Observations[(3)]	42^{+19}_{-7} (> 30)	1–6 (older?)	650	−6.07±0.03	
	Observations[(4)]	$38.1^{+1.7}_{-1.5}$	≳6			
	P2020	37	5	680	−5.84	0.087
			8	600	−6.07	0.086
	Present	37	5	673	−5.86	0.087
			8	593	−6.09	0.085
WISE J0720−0846B	Observations[(6)]	66±4	> a few	1250±40	−4.82±0.07	
	P2020	66	3	1324	−4.72	0.082
			4	1216	−4.88	0.082
	Present	66	3	1291	−4.78	0.081
			4	1201	−4.92	0.080
2M0805+48	Observations[(7)]	66^{+5}_{-14}	≥4			
2M1059−21	Observations[(7)]	67^{+4}_{-5}				
	P2020	66	5	1149	−4.99	0.080
			10	964	−5.33	0.077
	Present	66	5	1142	−5.02	0.079
			10	975	−5.33	0.076
Gliese 229 B	Observations[(8)]	71.4 ± 0.6	<10		−5.208 ± 0.007	
	P2020	70.5	8	1171	−4.99	0.078
			9	1140	−5.04	0.077
			10	1109	−5.09	0.077
	Present	70.5	8	1133	−5.06	0.077
			9	1103	−5.11	0.076
			10	1075	−5.16	0.076
		71.5	10	1110	−5.10	0.076

Notes. [(1)]Cheetham et al. (2018), [(2)]Chen et al. (2022), [(3)]Bowler et al. (2018), [(4)]Brandt et al. (2019), [(5)]Cardoso (2012), [(6)]Dupuy et al. (2019), [(7)]Sahlmann et al. (2020), [(8)]Brandt et al. (2021). Models are Phillips et al. (2020, P2020) and present calculations. We have taken 1 $M_{\rm Jup} = 9.5 \times 10^{-4}\ M_\odot$ in the evolutionary models.

and the present ones, with the CD21 EOS. Both models use the same abundances for helium, $Y = 0.275$, and metals, $Z_\odot = 0.017$, yielding an 'equivalent' helium abundance of $Y_{\rm eq} = 0.292$. This comparison highlights the impact of the H–He interactions in the most recent EOS models. As seen in the table, although the models including the new EOS yield temperatures cooler and luminosities fainter than the Baraffe et al. (2003) and Phillips et al. (2020) models for the relevant mass and age range, relieving part of the tension, it is clear that they are still far from resolving the disagreement with the observational determinations.

As noted by Cheetham et al. (2018), this discrepancy may be caused by the object being an unresolved binary BD system

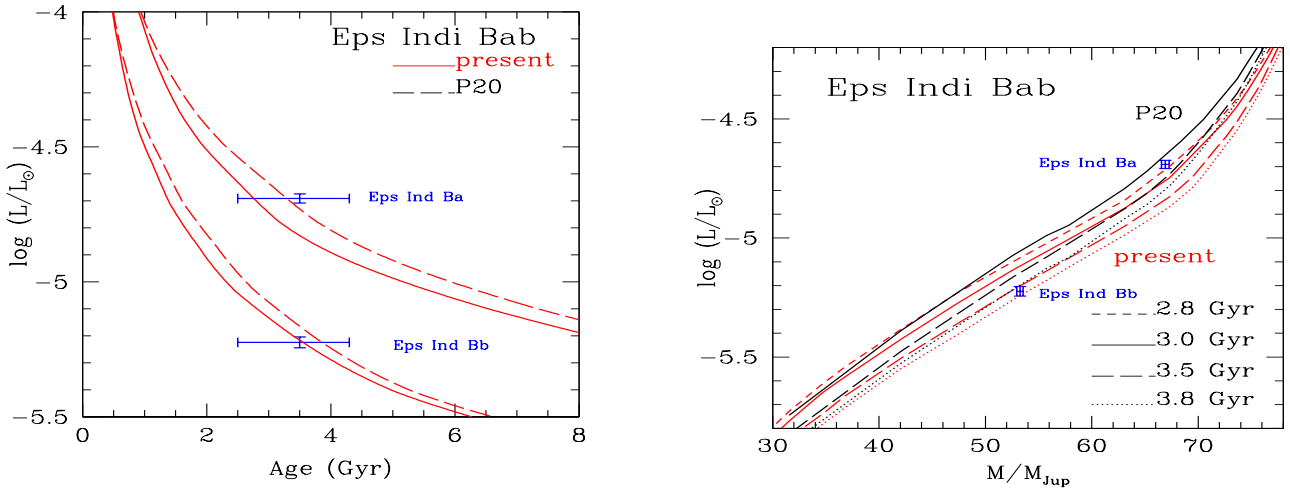

Fig. 4. Left: cooling curves for a 67 $M_{\rm Jup}$ (top) and a 53 $M_{\rm Jup}$ (bottom) BD, respectively, representative of the ϵ Ind Bab system. The solid line shows the present models based on the CD21 EOS; while the dashed line shows the Phillips et al. (2020) models based on the CMS19 EOS. Right: BD isochrones typical of the inferred age of the ϵ Ind Bab system, calculated with the present (red) and Phillips et al. (2020) (black) models.

or by the presence of an additional object in the system, which could have biased the RV data and caused an overestimate of the dynamical mass. An equal-mass binary of 500–600 K objects with $R \sim 1\,R_{\rm Jup}$, would, notably, provide a good match to the observed data while being in good agreement with the model predictions, namely $T_{\rm eff} = 600 \pm 40$ K for a 33 $M_{\rm Jup}$ object at 5 ± 1 Gyr (e.g., Phillips et al. 2020 or present models).

3.2. Eps Indi Bab

Recently, Chen et al. (2022) reported dynamical masses for the binary BD system ϵ Indi Ba ($Sp = T1 - 1.5$) and ϵ Indi Bb ($Sp = T6$, also called ϵ Indi C), with individual masses of $M_{\rm dyn} = 66.92 \pm 0.36\,M_{\rm Jup}$ and $M_{\rm dyn} = 53.25 \pm 0.29\,M_{\rm Jup}$, respectively, with a ≈5% precision. With an age of $3.5^{+0.8}_{-1.0}$ Gyr as derived from the activity of ϵ Indi A, this system provides a stringent constraint for BD cooling models, notably for old, massive BDs. Field-aged objects of spectral types T1 and T6 have effective temperatures in the range $T_{\rm eff} \simeq 1300$–900 K (e.g., Filippazzo et al. 2015). This is consistent with the inferred temperatures for Indi B and C, of namely $T_{\rm eff} \simeq 1300$–1340 K and $T_{\rm eff} \simeq 880$–940 K, respectively (King et al. 2010). Correct theoretical evolutionary models must therefore allow these objects to reach these spectral types and temperatures within the aforementioned timescale for the observed metallicity of the host star ϵ Indi A ([Fe/H] = 0.13). None of the widely used Chabrier & Baraffe (2000), Burrows et al. (2001), and Saumon & Marley (2008) 'cloudy' models can fullfill this constraint, and predict excessive temperatures and luminosities. The 'COND' models of Baraffe et al. (2003) predict faster cooling rates because of the less opaque atmospheres. However, as noted in Sect. 2, the lower opacity in the COND atmosphere models stems, notably, from missing line opacities. Therefore, this analysis suggests that the aforementioned models underpredict the cooling rates for ϵ Indi Ba and Bb.

Figure 4 displays the L–t and L–M relationships obtained for this system with the Phillips et al. (2020) cooling models, which are based on the CMS19 H/He EOS, and the present ones, which are based on the CD21 EOS, using the same ATMO atmosphere models and effective helium+heavy element abundance $Y_{\rm eff} = 0.292$. Here, we see that the Phillips et al. (2020) models yield an age of between ∼3.0 and 3.8 Gyr for the system for the observed luminosities, and the present model predicts slightly younger ages of 2.8 Gyr for Ba and 3.5 Gyr for Bb. Both models are in good agreement with the observational determination. Assuming coevality, this corresponds to a ∼0.7 Gyr uncertainty on the age of these BDs for this age and mass range. As seen in Fig. 13 of Chen et al. (2022), the Saumon & Marley (2008) hybrid models predict a significantly older age (5 Gyr) for the system, at odds with the observational determination, suggesting an overly slow cooling rate for these models. The corresponding effective temperatures and surface gravities between 2.8 and 3.5 Gyr with the present models are $T_{\rm eff} = 1354$–1265 K and $\log g = 5.45$ for ϵ Indi Ba, for a mass of 67 $M_{\rm Jup}$, and $T_{\rm eff} = 1060$–998 K and $\log g = 5.34$ for ϵ Indi Bb, for a mass of 53 $M_{\rm Jup}$ (see Table 2). As illustrated in Fig. 4 and discussed earlier, the faster cooling rate found for the most massive BDs with the CD21 EOS than with the CMS19 one stems from the sharp increase in the degeneracy in this mass range (see e.g., Fig. 1 of Chabrier & Baraffe 2000). The cooling rate then appears to be slightly too low as a function of the mass, with $\Delta \log L/\Delta \log M \simeq 3.95$ instead of 5.37 between ϵ Indi Ba and Bb, that is, from early T to late T, even though the discrepancy remains within 2σ. As mentioned earlier, this is more likely to stem from remaining issues with the atmosphere models than with the EOS.

3.3. Gl 758 B

Combining radial velocity and astrometry, Bowler et al. (2018) determined a dynamical mass of $M_{\rm dyn} = 42^{+19}_{-7}\,M_{\rm Jup}$ for the T7-T8 BD Gl 758 B, with a robust lower limit of 30.5 $M_{\rm Jup}$ at the 4σ level, for nominal ages of 1–6 Gyr adopted for the host star (Vigan et al. 2016). More recently, using HIPPARCOS and *Gaia* data, Brandt et al. (2021) derived the most precise mass measurement to date for this system, with $M_{\rm dyn} = 38.1^{+1.7}_{-1.5}\,M_{\rm Jup}$, while their analysis of activity and rotation of Gl 758A favours an age of $\gtrsim$6 Gyr. As for the objects we have examined in the previous sections, substellar evolutionary models generally underestimate the mass of Gl 758 B. As noted by the authors mentioned above, this discrepancy can be reconciled if the system is older, which is consistent with activity indicators and recent isochrone fitting of the host star, or alternatively if the models are systematically overluminous by ≈0.1–0.2 dex.

Atmospheric model fitting yields a bolometric luminosity $\log(L/L_\odot) = -6.07 \pm 0.03$, $T_{\rm eff} = 650$ K, and $\log g = 5.0$ for Gl 758 B. All current models essentially under-predict the mass for an age of 1–6 Gyr, or, alternatively, are overluminous by >0.1 dex at this age. This is in the opposite sense to results by Dupuy et al. (2009, 2014), who found that substellar cooling models under-predict the luminosities of BDs with dynamical masses by ≈0.2–0.4 dex. Altogether, the most likely explanation for the disagreement in mass probably resides in the age of Gl 758. Older ages of 6–9 Gyr would readily put the predicted and dynamical distributions in excellent agreement and are indeed suggested from the low activity level, lack of X-ray emission, and slow projected rotational velocity (see Bowler et al. 2018 and references therein). Indeed, more recent isochrone fittings are converging on an older value that agrees better with activity indicators, with an average of 5.3−7.5 Gyr (Brewer et al. 2016; Luck 2017). This is supported by the results displayed in Table 2, with the new models yielding a nearly perfect agreement with the observations for a mass of ∼30−40 $M_{\rm Jup}$ and an age of ∼5–8 Gyr.

3.4. WISE system J072003.20

Individual dynamical masses for the nearby M9.5+T5.5 binary system WISE J0720−0846AB were determined by Dupuy et al. (2019). The BD companion has a mass of $M_{\rm dyn} = 66 \pm 4\,M_{\rm Jup}$, an effective temperature of $T_{\rm eff} = 1250 \pm 40$ K, and a luminosity of $\log(L/L_\odot) = -4.8 \pm 0.15$. This suggests an age of greater than a few gigayears, which is consistent with the age estimates for the primary star. As shown in Table 2, both the P2020 and present models lead to nearly perfect agreement with the observational determinations for an age of ∼3–4 Gyr, with the new ones predicting a slightly younger age (more rapid cooling). For the primary star, WISE J0720−0846A, as noted in Dupuy et al. (2019), models (BHAC 2015) overestimate the luminosity for its mass ($M_{\rm dyn} = 99 \pm 6\,M_{\rm Jup}$), or conversely underestimate its mass for its luminosity, at about 2σ (see their Table 5 and Fig. 7). As mentioned above, the new CD21 EOS does not significantly change this analysis for such high (stellar) masses (see Table 1).

It is worth noting that the mass and age determinations for WISE J0720-0846B are very similar to those for the BD HD4747B ($66 \pm 3\,M_{\rm Jup}$, $2.9^{+0.5}_{-0.4}$ Gyr, $\log(L/L_\odot) = -4.55 \pm 0.08$; Brandt et al. 2021, Table 10), with which the present models are in very good agreement (see Table 2).

3.5. 2M1059 and 2M0805

Sahlmann et al. (2020) measured the complete astrometric orbits for the systems 2M0805+48 and 2M1059-21. These authors find a mass of $M_{\rm dyn} = 66^{+5}_{-14}\,M_{\rm Jup}$ and a spectral type of T5.5 for 2M0805+48 B and $M_{\rm dyn} = 67^{+4}_{-5}\,M_{\rm Jup}$ and T3.5 for 2M1059-21 B.

The striking feature of the analysis of these latter authors is that the mass for the T3.5 2M1059-21B object is significantly higher than its two spectral-type equivalents DENIS J2252-1730B (T3.5), $41 \pm 4\,M_{\rm Jup}$, and 2MASS J1534-2952A (T4.5), $51 \pm 5\,M_{\rm Jup}$. As noted by the authors, the mass of 2M0805+48B is almost equal to that of WI0720-08B estimated by Dupuy et al. (2019), which has the same spectral type, yet a mass higher than the other three T5 dwarfs with measured dynamical masses, which all have masses of $<61\,M_{\rm Jup}$ as an upper limit (see Table 6 of Dupuy et al. 2019). As shown by the authors (see their Fig. 13), the masses derived for each member of our two pairs are compatible at the 1σ level with the 5–12 Gyr isochrones of Baraffe et al. (2015), while >1 Gyr isochrones show reasonable agreement with the observational data.

This, as in the other previous analysis, highlights the fact that the higher observational masses than other T-dwarfs of similar spectral type and than predicted by the models – suggesting that models under-predict the mass for a given temperature or luminosity – predominantly concerns the most massive ($\gtrsim 60\,M_{\rm Jup}$) BDs, which are old enough to have reached the T spectral type domain, that is, older than $\gtrsim$1 Gyr for these masses. This strengthens our suggestion that this property stems mostly from the higher degeneracy, and therefore the faster cooling of these objects, which culminates at the highest central density of the stellar–substellar domain (see Fig. 1 of Chabrier & Baraffe 2000). The new models predict cooler temperatures and fainter luminosities for a given mass and age compared with the Baraffe et al. (2003) models, by up to about 100–150 K and ∼0.2−0.3 dex for the present ones, resolving at least partly the discrepancies mentioned above (see Table 2). Here again, we note that the mass and age of this system are similar to those of the BD HD19467B listed in Brandt et al. (2021), which is in excellent agreement with the models presented here.

3.6. Gliese 229B

Combining Keck/HIRES radial velocities, imaging with HiCIAO/Subaru and the HST, and absolute astrometry from Hipparcos and *Gaia*, Brandt et al. (2020) measured a dynamical mass of $M_{\rm dyn} = 70 \pm 5\,M_{\rm Jup}$ for the T7 BD Gliese 229B. Not only is this value higher than the $\simeq 64.0^{+2}_{-1}\,M_{\rm Jup}$ predicted by the Baraffe et al. (2003) or Saumon & Marley (2008) models for such a low luminosity, of namely $\log(L/L_\odot) = -5.208$, but to be compatible with the observational determinations, the models would predict an age of 7–10 Gyr. Such an age seems to be excluded by kinematic and activity indicators that rather suggest the range 2–6 Gyr. Gliese 229B therefore joins the club of ultracool BDs near the HBMM that are too massive, given their age, for the model predictions. For a 70 $M_{\rm Jup}$ at an age of 10 Gyr, the Phillips et al. (2020) models (see their Fig. 8), calculated with the Chabrier et al. (2019) EOS, are ∼0.1 dex less luminous than the Baraffe et al. (2003, B03) and ∼0.4 dex less luminous than the hybrid cloud tracks of SM08, helping to relieve some of the tension. As seen in Table 2, the present models, based on the new CD21 EOS, predict $\gtrsim$40 K cooler and ∼−0.1 dex fainter models than the Phillips et al. (2020) ones for mass and luminosity consistent with the latest observationally inferred values, for an age of about 9–10 Gyr, improving the agreement between models and observations.

Atmosphere models that show a good fit to the observed spectrum of Gliese 229B by Nakajima et al. (2015) yield acceptable solutions in the ranges $750\,{\rm K} \leq T_{\rm eff} \leq 900\,{\rm K}$ and $4.75 \leq \log g \leq 5.0$. As seen in Table 2, these values are relatively small compared to those from the models. However, it must be stressed that this fitting procedure is based on one single source of 'cloudy' atmosphere models, namely those of Tsuji (2002, 2005). A more robust determination of the effective temperature and gravity requires further detailed comparisons with more recent atmosphere models, a point we stress in Sect. 2.

Finally, we note that one possible scenario that would resolve the discrepancy between models and observations for Gl229 B is that this latter is itself an unresolved tight binary (see e.g., Brandt et al. 2021).

A similar case to Gliese 229B is HR 7672 B, with a dynamical mass of $M_{\rm dyn} = 72.7 \pm 0.8\,M_{\rm Jup}$ and a weighted average

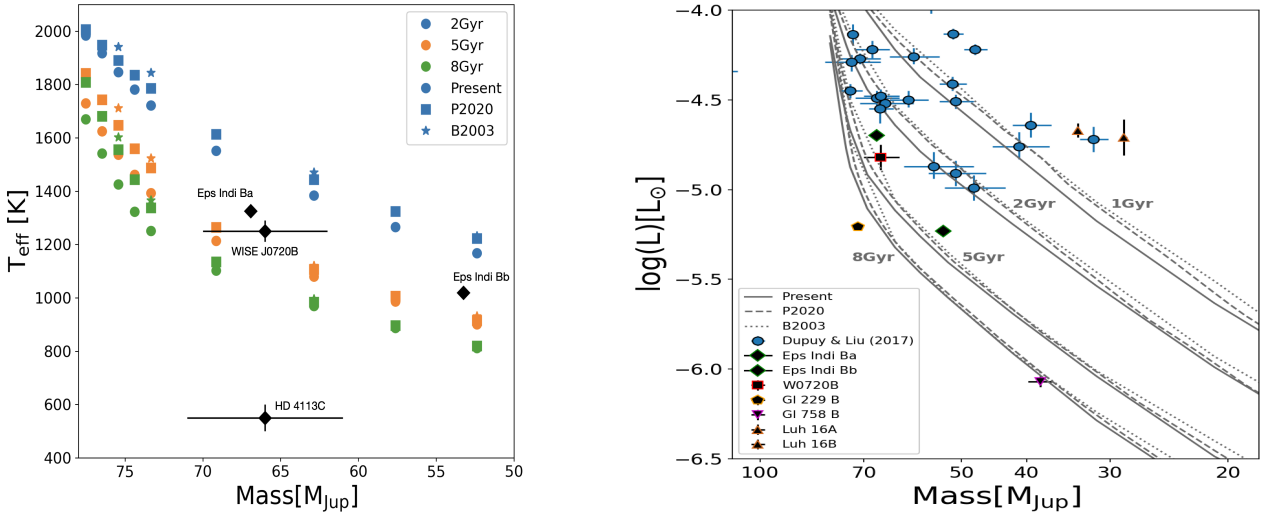

Fig. 5. Left: effective temperature as a function of mass for massive BDs for three isochrones, calculated with the present models based on the CD21 EOS and ATMO atmosphere models; the Phillips et al. (2020) models based on the CMS19 EOS and ATMO atmosphere models; and the Baraffe et al. (2003) models based on the SCvH EOS and the COND atmosphere models. Right: luminosity as a function of mass for three isochrones for BDs with dynamical mass measurements. References for the data are given in Table 2. All models have an equivalent helium mass fraction of $Y_{\rm eq} = 0.292$.

luminosity of $\log(L/L_\odot) = -4.25 \pm 0.05$ (Brandt et al. 2021), while the activity analysis suggests a rather young age, centred around 2 Gyr (Brandt et al. 2019, 2021). For this age and a mass of $M = 70\,M_\odot (= 72.7\,M_{\rm Jup})$, the present models predict $\log(L/L_\odot) = -4.25$ and $T_{\rm eff} = 1730$ K, while the Phillips et al. (2020) ones yield $\log(L/L_\odot) = -4.16$ and $T_{\rm eff} = 1785$ K.

In order to illustrate the results listed in Table 2, Fig. 5 displays the $T_{\rm eff}$–mass and L–mass data comparisons (as in Fig. 8 of Phillips et al. 2020), including the most recent determinations, for massive BDs for four isochrones, namely 1, 2, 5, and 8 Gyr, based on the CMS19 (Phillips et al. 2020) and CD21 (present) EOS models.

To briefly summarise this section, we note that the models based on the most recent EOSs, notably the latest CD21 one, reach cooler temperatures and fainter luminosities than the previous generation for a given mass and age, illustrating the faster cooling rates for massive, old ($\gtrsim$1 Gyr) BDs. In general, these lead to much better agreement with the observational determination. As seen in Table 2, some tension potentially remains for Gl229B but most importantly for HD4113C, which appears to be substantially cooler and fainter than predicted by the models. Given the general agreement for all the other objects, this suggests that these two BDs could be unresolved systems.

4. Conclusion

In this study, we explored the impact of the latest EOS for dense hydrogen–helium mixtures on the structure and evolution of very low-mass stars and BDs. Whereas the previously used Saumon et al. (1995) and Chabrier et al. (2019) EOSs are based on the so-called additive volume law, which implies that the interactions between hydrogen and helium species are not taken into account, these interactions are included in the Chabrier & Debras (2021) EOS based on the QMD simulations of Militzer & Hubbard (2013) (see CD21 for details). These interactions modify the thermodynamic properties of the H–He mixture in two ways. They yield cooler and denser and therefore more compact structures, that is, smaller radii and therefore fainter luminosities for given masses and ages. They also yield cooler entropy profiles, a quantity of prime importance for these fully convective bodies, which affects the onset and the development of electron degeneracy throughout the body (see Fig. 9 of CD21). This translates into faster cooling rates and therefore larger masses for given effective temperatures and luminosities at a given age in the BD regime (see Table 2). Confronting these new models with several observationally determined BD dynamical masses, we show that this does indeed improve the agreement between evolutionary models and observations and resolves at least part of the observed discrepancy for massive, rather old BDs. In the stellar domain, the impact of the new EOS is inconsequential. Resolving the remaining discrepancies between BD observations and models probably requires further improvements of atmosphere models and self-consistent evolutionary calculations with these models. Work in this direction is in progress.

A noticeable consequence of this improvement in the dense H–He EOS is that it yields a larger H-burning minimum mass, now found to be $0.075\,M_\odot$ ($\sim 78\,M_{\rm Jup}$) with the ATMO atmosphere models for solar helium and heavy element abundances, $Y = 0.275$, $Z_\odot = 0.017$, respectively, and therefore an equivalent helium abundance $Y_{\rm eq} \simeq Y + Z = 0.292$. The corresponding radius, effective temperature, and luminosity at 10 Gyr are listed in Table 1. These new BD models will be available online[1,2].

Acknowledgements. The authors are grateful to the referee, Timothy Brandt, whom remarks helped clarifying the manuscript. This work has been supported by the consolidated STFC Consolidated Grant ST/V000721/1, the ERC grant No. 787361-COBOM and the Programme National de Planétologie (PNP).

References

Allard, F., Homeier, D., Freytag, B., & Sharp, C. M. 2012, in Low-Mass Stars and the Transition Stars/Brown Dwarfs, eds. C. Reylé, C. Charbonnel, & M. Schultheis (Les Ulis: EDP Sciences), EAS Publ. Ser., 57, 3
Allard, F., Homeier, D., Freytag, B., et al. 2013, MSAIS, 24, 128
Baraffe, I., Chabrier, G., Barman, T. S., et al. 2003, A&A, 402, 701
Baraffe, I., Homeier, D., Allard, F., & Chabrier, G. 2015, A&A, 577, A42

[1] http://perso.ens-lyon.fr/isabelle.baraffe/CBPD2022
[2] http://opendata.erc-atmo.eu

Bowler, B. P., Dupuy, T. J., Endl, M., et al. 2018, AJ, 155, 159
Brandt, T. D., Dupuy, T., & Bowler, B. 2019, AJ, 158, 140
Brandt, T. D., Dupuy, T. J., Bowler, B. P., et al. 2020, AJ, 160, 196
Brandt, G. M., Dupuy, T. J., Li, Y., et al. 2021, AJ, 162, 301
Brewer, J. M., Fischer, D. A., Valenti, J. A., et al. 2016, ApJS, 225, 1
Burrows, A., Marley, M., Hubbard, W. B., et al. 1997, ApJ, 491, 856
Burrows, A., Hubbard, W. B., Lunine, J. I., & Liebert, J. 2001, Rev. Mod. Phys., 73, 719
Caffau, E., Ludwig, H.-G., Steffen, M., & Freytag, B.,& Bonifacio, P., 2011, Sol. Phys., 268, 255
Cardoso, C. 2012, PhD Thesis, Univ. Exeter, UK
Chabrier, G., & Baraffe, I. 2000, ARA&A, 38, 337
Chabrier, G., & Debras, F. 2021, ApJ, 917, 4
Chabrier, G., & Potekhin, A. 1998, Phys. Rev. E, 58, 4941
Chabrier, G., Baraffe, I., Allard, F., & Hauschildt, P. 2000, ApJ, 542, 464
Chabrier, G., Baraffe, I., Leconte, J., et al. 2009, in 15th Cambridge Workshop on Cool Stars, Stellar Systems, and the Sun, ed. E. Stempels (Melville, NY: AIP), AIP Conf. Ser., 1094, 102
Chabrier, G., Mazevet, S., & Soubiran, F. 2019, ApJ, 872, 51
Cheetham, A., Ségransan, D., Peretti, S., et al. 2018, A&A, 615, 160
Chen, M., Li, Y., Brandt, T. D., et al. 2022, AJ, 163, 288
Dieterich, S. B., Henry, T. J., Jao, W.-C., et al. 2014, AJ, 147, 94
Dieterich, S. B., Weinberger, A. J., Boss, A. P., et al. 2018, ApJ, 865, 28
Dupuy, T., Liu, M. C., Bowler, B. P., et al. 2009, ApJ, 706, 328
Dupuy, T., Liu, M. C., Ireland, M. J., et al. 2014, ApJ, 790, 133
Dupuy, T., Liu, M. C., Best, W. M. J., et al. 2019, AJ, 158, 174
Filippazzo, J. C., Rice, E. L., Faherty, J., et al. 2015, ApJ, 810, 158
King, R. R., McCaughrean, M. J., Homeier, D., et al. 2010, A&A, 510, 99
Luck, R. E. 2017, AJ, 153, 1
Militzer, B., & Hubbard, W. B. 2013, ApJ, 774, 148
Morley, C., Fortney, J., Marley, M. S., et al. 2012, ApJ, 756, 172
Morley, C., Marley, M. S., Fortney, J., et al. 2014, ApJ, 787, 78
Mowlavi, N., Eggenberger, P., Meynet, G., et al. 2012, A&A, 541, 41
Nakajima, T., Tsuji, T., & Takeda, Y. 2015, AJ, 150, 53
Phillips, M., Trembin, P., Baraffe, I., et al. 2020, A&A, 637, 38
Sahlmann, J., Burgasser, A. J., Bardalez Gagliuffi, D. C., et al. 2020, MNRAS, 495, 1136
Saumon, D., & Marley, M. 2008, ApJ, 689, 1327
Saumon, D., Chabrier, G., & vanHorn, H. 1995, ApJS, 99, 713
Tremblin, P., Amundsen, D. S., Mourier, P., et al. 2015, ApJ, 804, L17
Tremblin, P., Amundsen, D. S., Chabrier, G., et al. 2016, ApJ, 817, L19
Tremblin, P., Chabrier, G., Baraffe, I., et al. 2017, ApJ, 850, 46
Tremblin, P., Padioleau, T., Phillips, M. W., et al. 2019, ApJ, 876, 144
Tsuji, T. 2002, ApJ, 575, 262
Tsuji, T. 2005, ApJ, 621, 1033
Vigan, A., Bonnefoy, M., Ginski, C., et al. 2016, A&A, 587, A55